Annealing effect on corrosion resistance of $Bi_xTi_yO_z$ coatings

M.J. Pinzón[a,b], J.E. Alfonsoa[a,c,*], J.J. Olaya[a,b], and C.A. Pineda-Vargas[d,e]
[a]*Grupo de Ciencia de Materiales y Superficies,*
Universidad Nacional de Colombia, Bogotá AA 14490, Colombia
[b]*Departamento de Ingeniería Mecánica y Mecatrónica,*
Universidad Nacional de Colombia, Bogotá AA 14490, Colombia
[c]*Associate Researcher of Centro Internacional de Física,*
Bogotá AA 14490, Colombia
**e-mail: jealfonsoo@unal.edu.co*
[d]*Materials Research Department,*
iThemba LABS, PO Box 722 Somerset West 7129, South Africa.
[e]*Faculty of Health & Wellness Sciences,*
CPUT, PO Box 1906 Bellville 7535, South Africa.

Received 29 July 2015; accepted 13 May 2016

Bismuth titanate ($Bi_xTi_yO_z$) has received widespread attention due to the fact that during recent times it has found important applications in strategic research fields such as optics and optoelectronic, and more recently studies have shown how their physicochemical properties may be harnessed in order to be able to use $Bi_xTi_yO_z$, as an anticorrosive coating. In this work bismuth titanate ($Bi_xTi_yO_z$) coatings were grown on titanium alloy (Ti6Al4V) substrates, using RF magnetron sputtering at room temperature. The main objectives of the work were quantify the evolution of crystallographic phase formation, as a function of the annealing temperature, and establish the chemical composition in order to characterize the behavior of the bismuth titanate coating as a protective coating of the corrosion. The morphology of the coating was observed via Scanning Electronic Microscopy (SEM); the crystalline structure was characterized by X-ray Diffraction (XRD) and the chemical composition was analyzed by Rutherford Backscattering Spectrometry (RBS). The corrosion resistance of the coatings was studied by Potentiodynamic polarization (PP) test (Tafel extrapolation). SEM results showed that the surface roughness of the coatings changed when the temperature of annealing increased. Similar change occurred after PP tests. The XRD analysis revealed a change in the coatings microstructure as a function of the annealing temperature, since they evolved from a completely amorphous phase to a polycrystalline phase. RBS results indicate that coatings growing at high temperature have a complex chemical composition. Finally, the electrochemical analysis showed that the corrosion resistance of the coating is much better in the amorphous phases of bismuth titanate than in the polycrystalline phases.

Keywords: Annealing; bismuth titanate; corrosion; Tafel extrapolation; potentiodynamic polarization; polarization resistance; X-Ray diffraction; Rutherford backscattering.

PACS: 81.15.Cd; 81.40.Ef; 81.65.Kn; 82.45.Bb; 82.80.Yc

1. Introduction

Because of their many electrical, optical, ferroelectric, and dielectric properties, and due to their friendly behavior within the environment, bismuth titanate compounds have become a family of a very interesting materials for various applications, such as non-volatile random access memories, photocatalysts, and optoelectronic, piezoelectric, and pyroelectric devices [1-5]. This family ($Bi_xTi_yO_z$) consists of several crystalline structures, such as sillenite ($Bi_{12}TiO_{20}$), aurivillius (Layered-Perovskite, $Bi_4Ti_3O_{12}$), the meta-stable $Bi_2Ti_4O_{11}$ phase and pyrochlore ($Bi_2Ti_2O_7$), as well as the amorphous phase [6-12]. For instance, the aurivillius phase exhibits monoclinic symmetry beneath its Curie temperature (948 K), which allows it to exhibit two possible directions of polarization, which makes it very interesting for optical applications; furthermore, its piezoelectricity and ferroelectricity make it a suitable candidate for the development of devices such as transductors and actuators, in addition to its use in the automotive, aeronautic, and aerospace industries [9]. Additional research shows that this compound exhibits reversible polarization, a high dielectric constant, and electro-optic switching behavior, which makes it the subject of special attention for applications such as non-volatile memories, capacitors of dynamic random-access memories, optical displays, and pyroelectric devices [13-14]. Meanwhile, the sillenite structure has photorefractive and photoconductive properties, which make it an optically active material and allow it to exhibit electro-optic, piezoelectric, and elasto-optic effects that are interesting for use in optical memories and dynamic holography [15-16], and also it also exhibits great photocatalytic activity in the region of UV radiation for reactions such as the photo-degradation of methyl orange [17]. On the other hand, the pyrochlore structure has optical properties such as photocatalytic activity in the degradation of Rhodamine B under visible-light; other studies done on this compound have proposed it as a material for use in the fabrication of advanced MOSFET transistors, taking advantage of its permittivity (relatively high) and low current leakage [18-19].

$Bi_2Ti_4O_{11}$ is a meta-stable phase of the bismuth titanate, which, although difficult to synthesize, has been the subject of several investigations aimed at studying its antiferroelectric, dielectric, and microwave dielectric properties [6,20].

The above information about the many investigations performed on the bismuth titanate family compounds shows that they have been focused on the study of the structural behavior, optical properties, and electrical properties, which has resulted in there being few studies or information about the behavior of these compounds in corrosive environments or possible biological applications. For this reason, in the present paper we present the results of the evaluation of the corrosion resistance of bismuth titanate coatings grown on titanium alloy substrates Ti6Al4V at room temperature and then with a annealing at 673 K and 973 K.

2. Experimental

2.1. Materials

The coatings were grown from a target of $Bi_4Ti_3O_{12}$ (Plasma Materials, 99.9% purity) with dimensions of 101.6×6.35 mm. Titanium alloy (Ti6Al4V) disks with dimensions 14×2 mm were used as substrates. The potentiodynamic polarization tests were carried out in a 3.5% NaCl solution.

2.2. Equipment

For developing this research, a Branson 3510 ultrasonic washer was employed for the cleaning of the substrates, an Alcatel HS 2000 RF sputtering system for growth of the films, a Heraus furnace for annealing the samples, a Panalytical X'Pert PROX Ray diffractometer (XRD) for observing the evolution of the crystalline structure, a Gamry Instruments reference 600 potentiostat/galvanostat accompanied by three electrode cells composed of a Satured Calomel Electrode (S.C.E.) as a reference electrode, a Platinum auxiliary electrode as a counter electrode, and the substrates as a working electrode, in order to obtain the polarization curves, and Gamry Echem Analyst software was employed for carrying out the analysis of the polarization curves.

2.3. Substrates preparation

The substrates were obtained from a rod of titanium alloy (Ti6Al4V), which was cut in disks through a wire erosion process. These disks were sanded with silicon carbide sandpapers of 220 to 1200 grit, and then polished with a rotating polishing cloth impregnated with alumina in order to generate a specular surface. Finally, the substrates were cleaned by mean ultrasonic immersion in isopropyl alcohol, acetone, and distilled-deionized water.

2.4. Sputtering deposition and annealing

The samples were placed into the vacuum chamber of the Alcatel sputtering system, which was subject to a process of vacuum generation through of a mechanical pump and a pressure of 5.4 Pa was achieved; then the high vacuum generation was begun through use of a turbomolecular pump, with which a base pressure of 4×10^{-3} Pa was achieved. The next step was to insert Argon with a constant flow of 20 sccm until achieving the working pressure (7.4×10^{-1} Pa). Then the RF source at 150 W of power supplied to the target was activated, at which moment the deposition was started, which lasted 1 hour. The substrates were kept at room temperature (RT) during the deposition process, and the target-substrate distance was 55 mm. Then the annealing process was carried out in a Heraus furnace, in which the samples were in an oxygen atmosphere that entered with a flow of 5.6 mL/min. The treatment lasted 1 hour, with an increase time of 2 hours from room temperature until reaching each of the temperatures studied (673 K and 973 K).

2.5. X-ray diffraction and evaluation of the corrosion resistance

The samples before and after the annealing were characterized by means of X-ray diffraction in Bragg-Brentano geometry with Cu-kα radiation ($\lambda = 1.5405$ Å) in the range between 25 and 80° in steps of 0.02°. The potentiodynamic polarization tests were carried out by placing the samples in the three electrode cells and exposing an area 0.159 cm^2 to the 3.5% NaCl solution. Then there was a wait of 1 hour before starting the test, in order to allow the stabilization of the solution; this procedure was carried out in a Faraday cage in order to eliminate the effects of the noise produced by the stationary electric fields around the cell tests. The test started at room temperature, in a range between -300 and 400 mV with respect to the open circuit potential, with a scan rate of 0.5 mV/s. The measurements obtained in the potentiodynamic polarization tests were analyzed with Gamry Echem Analyst software and the Tafel extrapolation method [21].

2.6. Rutherford Backscattering Spectrometry

Characterization of the chemical composition and thicknesses of thin deposits was carried out by Rutherford Backscattering Spectrometry (RBS). Measurements were performed using a 2.0 MeV mono-energetic $^4He^+$ ion beam, delivered by the 6.0 MV Single Ended Van de Graaff accelerator at iThemba LABS, South Africa. The samples were bombarded for a duration of about 10 min using a beam current of $\sim$50 nA. The backscattered $^4He^+$ ions were detected in standard IBM geometry at 165° with respect to the incoming beam using a surface barrier detector (with 20 keV resolution) in a vacuum pressure of 5×10^{-6} mbar. The simulation of the RBS spectra was performed using the computer program RUMP.

TABLE I. Values of the corrosion parameters of the $Bi_xTi_yO_z$ coatings and the Ti6Al4V substrates.

Sample	E_{corr} (mV)	i_{corr} (A/cm^2)	β_a (V/decade)	β_c (V/decade)	R_p (Ω/cm^2)	Corrosion Rate (mμpy)
Substrate	-5.55E+01	1.29E-08	3.22E-01	2.12E-01	4.31E+06	1.12E+02
RT	-1.66E+01	7.26E-09	5.28E-01	3.13E-01	1.18E+07	6.35E+01
673 K	-1.91E+02	4.76E-08	1.16E+00	1.39E-01	1.13E+06	4.16E+02
973K	1.58E+02	2.40E-07	4.53E-01	2.75E-01	3.09E+05	2.10E+03

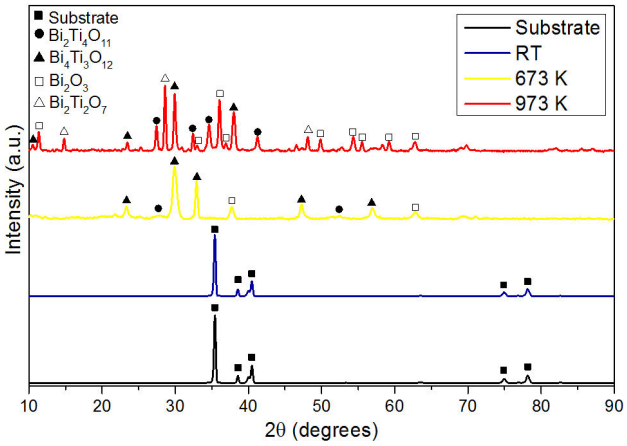

FIGURE 1. XRD patterns of $Bi_xTi_yO_z$ coatings and Ti6Al4V substrate.

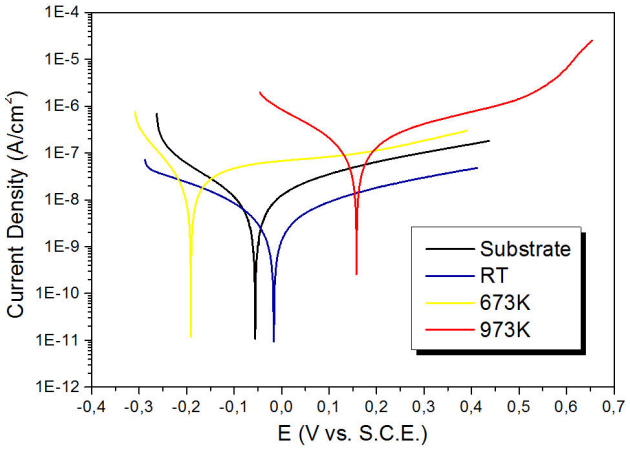

FIGURE 2. Polarization curves of $Bi_xTi_yO_z$ coatings and Ti6Al4V substrate.

2.7. Scanning Electron Microscopy

The surface morphology of the coatings was studied by imaging the secondary electrons with a Quanta 2000 scanning electron microscope operating at 15 kV and 10 mA.

3. Results and Discussion

Figure 1 shows the XRD pattern of substrate and coatings of bismuth titanate. It can be observed that the coating grown at room temperature without annealing is amorphous. Moreover, the coatings annealed at 673 K and 973 K exhibit several crystalline phases, *e.g.* at 673 K appears the Aurivillus structure of the compound $Bi_4Ti_3O_{12}$ (PDF 350795), the Meta-stable phase $Bi_2Ti_4O_{11}$ (PDF 150325) and some peaks of Bi_2O_3 (PDF 010712274), then, in the samples annealaed at 923K, persist the three aforementioned structures, and appear the Pyrochlore structure $Bi_2Ti_2O_7$ (PDF 320118).

Figure 2, shows the polarization curves obtained from the substrates and films, from which the Tafel slopes (β_a and β_c) and the corrosion current (icorr) were obtained, with which the polarization resistance (R_p) was calculated by means the Tafel equation [21]:

$$i_{corr} = \frac{1}{2.303R_p\left(\frac{1}{\beta_a} + \frac{1}{|\beta_c|}\right)} \quad (1)$$

The results shown in Table I allow establishing that polarization resistance of the amorphous coatings increased in

TABLE II. Stoichiometry for each layer as determined by RBS of $Bi_xTi_yO_z$ coatings grown at RT.

	Layer	Elements					Thickness (atoms/cm^2)
		Bi	Ti	O	V	Al	
	1	0.70	0.00	0.30	0.00	0.00	50
Un-	2	0.20	0.10	0.70	0.00	0.00	1295
corroded	3	0.00	0.85	0.00	0.10	0.05	30000
	1	0.70	0.00	0.30	0.00	0.00	65
Corroded	2	0.22	0.11	0.67	0.00	0.00	1250
	3	0.00	0.85	0.00	0.10	0.05	30000

TABLE III. Stoichiometry for each layer as determined by RBS of $Bi_xTi_yO_z$ coatings with a annealing at 673 K.

	Layer	Elements					Thickness (atoms/cm^2)
		Bi	Ti	O	V	Al	
Uncorroded	1	0.70	0.00	0.30	0.00	0.00	35
	2	0.27	0.13	0.60	0.00	0.00	100
	3	0.22	0.10	0.68	0.00	0.00	1150
	4	0.00	0.30	0.70	0.00	0.00	680
	5	0.00	0.55	0.45	0.00	0.00	1100
	6	0.00	0.70	0.00	0.09	0.21	30000
Corroded	1	0.70	0.00	0.30	0.00	0.00	53
	2	0.30	0.20	0.50	0.00	0.00	80
	3	0.24	0.10	0.66	0.00	0.00	1150
	4	0.00	0.30	0.70	0.00	0.00	500
	5	0.00	0.57	0.43	0.00	0.00	1100
	6	0.00	0.70	0.00	0.09	0.21	30000

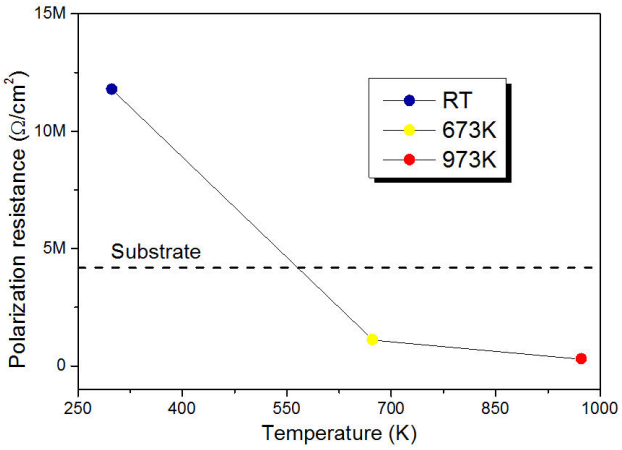

FIGURE 3. Behavior of the polarization resistance for coatings; the dashed line represent the polarization resistance of the substrate.

the best of cases to approximately 3 times the corrosion resistance with regard to bare substrate. Furthermore, it was also shown that the increase of the annealing temperature decreased the values of the polarization resistance to values below those of the substrate (see Fig. 3).

This behavior can be explained through the crystalline transition experienced by the coatings. This is because the annealing treatment probably produces cracks in the surface of the film through which the electrolyte penetrates to the substrate.

RBS analyses (Figs. 5-7, and Tables II-IV) of the BiTiO thin films growth at RT show that the chemical composition of both the corroded and uncorroded coatings did not have a significant change. particularly at the substrate-layer interface. There appear to be no mixing of the BiTiO deposit at the substrate interface and is mostly composed of Ti. RBS analyses of the systems grown at 673 K show a high degree

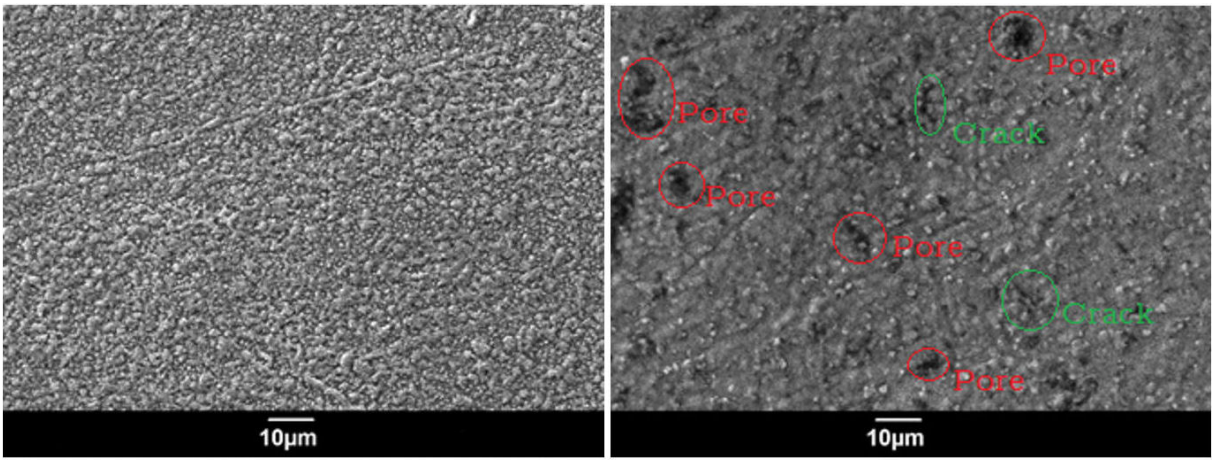

FIGURE 4. SEM micrographs of $Bi_xTi_yO_z$ coatings with a annealing at 973 K a) before corrosion test, b) after corrosion test.

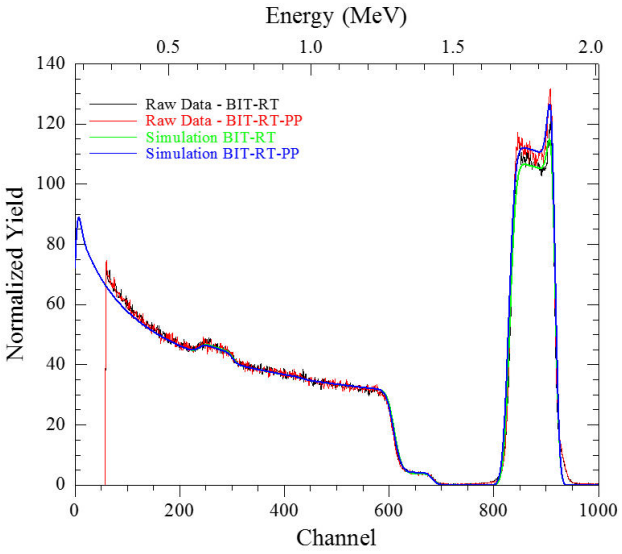

FIGURE 5. RBS pattern and simulation of BiTiO thin films grown at Room Temperature, before (green line) and after of corrosion test (blue line).

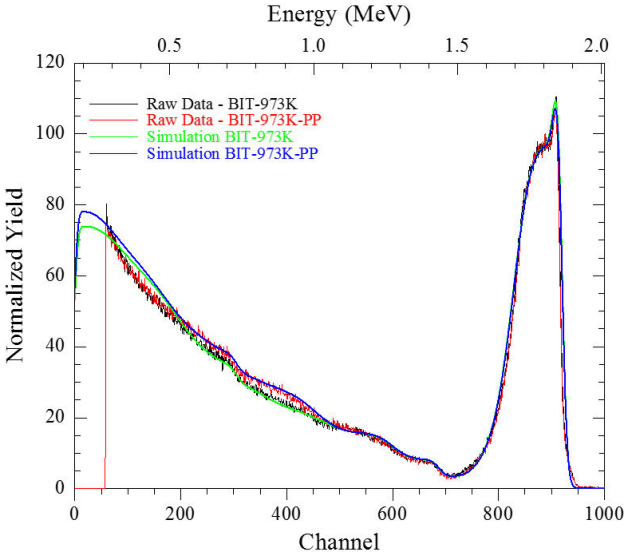

FIGURE 6. RBS pattern and simulation of BiTiO thin films grown at 673 K before (green line) and after of corrosion test (blue line).

of mixing at the interface with very little difference on the chemical composition between corroded and uncorroded TiAlV-BiTiO systems. However a higher oxygen content was detected on both cases. This result can be explained by considering that the oxygen of the solution (water +NaCl) could react with the titanium substrate. Additionally, be observed diffusion of Bi of the coating toward substrate when the annealing temperature increase that cause expansion tensions

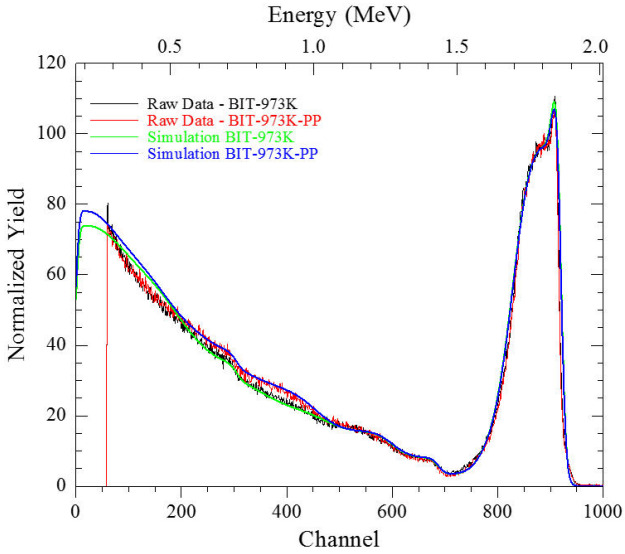

FIGURE 7. RBS pattern and simulation of BiTiO thin films grown at 973 K before (green line) and after of corrosion test (blue line).

between substrate and coating which produce more corrosion process in these coatings. This result can be explained by considering that the oxygen of the solution (water +NaCl) could react with the titanium substrate. Additionally, be observed diffusion of Bi of the coating toward substrate when the annealing temperature increase that cause expansion tensions between substrate and coating which produce more corrosion process in these coatings.

4. Conclusions

Amorphous $Bi_xTi_yO_z$ coatings were grown via rf magnetron sputtering on titanium alloy (Ti6Al4V) substrates. After a thermal treatment, the films evolved into polycrystalline structures. The evaluation of the corrosion resistance allowed establishing that it decreased in polycrystalline coatings and reached higher values in amorphous coatings. This behavior probably relates with diffusion process of Bi toward substrate, that present in coatings annealing at high temperatures that cause expansion tensions between substrate and coating.

Acknowledgments

The authors are grateful to “Patrimonio autónomo Fondo Nacional de Financiamiento para la Ciencia, la Tecnología y la Innovación Francisco José de Caldas” for the financial support grants, through to the0472-2013 proyect, to the Universidad Nacional de Colombia and iThembalabs.

1. O. Subohi, G.S. Kumar, M.M. Malik, R. Kurchania, *Opt.-Int. J. Light Electron Opt.* **125** (2014) 820-823.
2. P. Pookmanee, P. Boonphayak, S. Phanichphant, *Ceram. Int.* **30** (2004) 1917-1919.
3. O. Subohi, G.S. Kumar, M.M. Malik, *Opt.-Int. J. Light Electron Opt.* **124** (2013) 2963-2965.
4. J. Hou, S. Jiao, H. Zhu, R.V. Kumar, *J. Solid State Chem.* **184** (2011) 154-158.
5. O. Subohi, G.S. Kumar, M.M. Malik, R. Kurchania, *Phys. B Condens. Matter* **407** (2012) 3813-3817.
6. J. Liu, C.-G. Duan, W.-G. Yin, W.N. Mei, R.W. Smith, J.R. Hardy, *J. Chem. Phys.* **119** (2003) 2812-2819.
7. K. Sardar, R. I. Walton, *J. Solid State Chem.* **189** (2012) 32-37.
8. V.M. Skorikov, Y.F. Kargin, A.V. Egorysheva, V.V. Volkov, M. Gospodinov, *Single Crystals. Inorg. Mater*.**41** (2005) S24-S46.
9. T. Jardiel, A. Caballero, M. Villegas, *J. Ceram. Soc. Japan* **10** (2008) 511-518.
10. Y. Zhang, S.X. Shang, B.B. Huang, *Appl. Catal. B Environ.* **52** (2004) 109-116.
11. I.Radosavljevic, J. S. O. Evans, A.W. Sleight, *J. Solid State Chem.* **136** (1998) 63-66.
12. S. Kojima, *et al*., *J. Non. Cryst. Solids* **293-295** (2001) 250-254.
13. F. Soares-Carvalho, P. Thomas, *J. sol-gel Sci. Technol.* (1997) 759-763.
14. A. Umabala, M. Suresh, A. Prasadarao, *Mater. Lett.* **44** (2000) 175-180.
15. A.V. Egorysheva, *Inorg. Mater.* **45** (2009) 1175-1182.
16. N.C. Deliolanis, E.D. Vanidhis, N.A. Vainos, *Appl. Phys. B* **85** (2006) 591-596.
17. J. Hou, Z. Wang, S. Jiao, H. Zhu, J. Hazard, *Mater.* **192** (2011) 1772-9.
18. J. Hou, S. Jiao, H. Zhu, R.V. Kumar, *J. Solid State Chem.* **184** (2011) 154-158.
19. J. Harjuoja, S. Väyrynen, M. Putkonen, L. Niinistö, E. Rauhala, *J. Cryst. Growth* **286** (2006) 376-383.
20. B. Fu, Y. Zhang, M. Hong, F. Jiang, J. Cao, *J. Mater. Sci. Mater. Electron.* **24** (2013) 3240-3243.
21. E. McCafferty, *Corros. Sci.* **47** (2005) 3202-3215.